5 Particle Physics at DESY/HERA (H1)

L. Lindfeld (until December 2006), Katharina Müller, K. Nowak, P. Robmann, C. Schmitz, U. Straumann, P. Truöl, and Stefania Xella Hansen (until May 2006)

in collaboration with: N. Berger, M. Del Degan, C. Grab, G. Leibenguth, M. Sauter, A. Schöning, and T. Zimmermann, Institut für Teilchenphysik der ETH, Zürich; S. Egli, R. Eichler, M. Hildebrandt, and R. Horisberger, Paul–Scherrer–Institut, Villigen, and 37 institutes outside Switzerland

(H1 - Collaboration)

5.1 Electron-proton collisions at a centre of mass energy of 320 GeV - summary

On March 20, 2007 the last data were taken by the H1-collaboration from collisions of 27.4 GeV electrons and positrons with 920 GeV protons. For the remaining months until the end of the experimental phase on June 30, 2007 the HERA storage ring will run with protons at a reduced energy of 460 GeV. The H1-detector will then record events with triggers optimized for a measurement of the longitudinal structure function $F_L(x, Q^2)$ at high electron inelasticity. The integrated luminosity for the post-upgrade HERA-II phase (2004-2007) amounts to 238 pb^{-1} taken with electron and 219 pb^{-1} taken with positron beams, compared to 118 pb^{-1} in total for the HERA-I phase (1993-2000). During the last, low energy phase both left- and right-handed longitudinally polarized beams will be available with polarisations exceeding slightly those obtained during all of the HERA-II running. All runs up to the end are already included in the searches for beyond the Standard Model physics most readily accessible through the multi-lepton (electron or muon), high transverse momentum analysis (see Sec. 5.4.1 below).

As in the past both the H1- and the ZEUS-collaboration continued their efforts dedicated to the exploration of proton structure and tests of quantum chromodynamics (QCD) predictions, evidenced by a nearly constant publication rate over the years. This program entails the precise determination of the neutral and charged electroweak current cross sections at high momentum transfer leading to parton density functions in pre-HERA inaccessible domains of Bjorken x and momentum transfer Q^2, diffractively produced final states, hidden and open charm and beauty production as well as the already mentioned searches for states outside the Standard Model.

Our analysis effort concentrated on events with isolated photons produced in either photoproduction ($Q^2 \approx 0$) or deep inelastic scattering (DIS, $Q^2 > 4$ GeV^2) and search for lepton flavor violation. The thesis of Linus Lindfeld resulting from the latter project has been concluded (1) and a publication has been submitted (2). This work was described in last years annual report (3) in greater detail. The DIS part of isolated photon production, the thesis project of Carsten Schmitz supervised by Katharina Müller, is also concluded. Results have been presented at conferences, and the internal H1-reviewing process for the publication is nearly finished. Higher statistics and an extended kinematical range compared to earlier work allows a clear distinction of the radiation originating from the initial or final state leptons and the struck quarks and thus a test of QCD calculations carried out at the Institute of Theoretical Physics (UZH) (4). This is discussed in Sec. 5.4.2 below in more detail. Noteworthy is also the fact, that this will be

the first H1-publication using a major fraction of the HERA-II data, 227 pb^{-1} in total, about twice the hitherto largest published sample in any of the collaboration papers. First results of the photoproduction analysis, the thesis project of Krzysztof Nowak, are available, too. A short account of this work is also given below (Sec. 5.4.2).

Other analyses of HERA-I data lead to fourteen additional publications (5)-(18), of which three still being reviewed. As usual the preliminary results of ongoing analyses were presented at the summer 2006 high-energy physics conference ICHEP06 in Moscow (19) ((20)-(37)). The following subjects have been covered:

- searches for states and interactions outside the Standard Model like lepton flavor violation (1; 2), excited neutrinos (35), leptoquarks (36), multi-lepton events (33) and events with isolated leptons and missing transverse momentum (32; 35; 37) (see also Sec. 5.4.1 below), single top production (16), doubly charged Higgs bosons (9);

- searches for exotic baryons like strange pentaquarks (11), or decaying to $\Xi\pi$ (30);

- charged and neutral current interactions with longitudinally polarized electrons and positrons (28; 29), discussed in last years annual report (3);

- various aspects of diffraction like parton densities determined from dijet production and F_2^D (13; 18; 24; 25), DIS with the leading proton observed (12), charm in DIS and photoproduction (15; 31), elastic J/ψ production (5), and ρ_0 photoproduction (7; 27);

- final states involving heavy quarks like inclusive charm ($D^{*\pm}$) and beauty dijet production in DIS or at $Q^2 \approx 0$ (10; 14; 17);

- testing specific aspects of QCD based model calculations like isolated photon production (23), which was already mentioned, deeply virtual Compton scattering (26), dijet and threejet production (6; 14; 20) as well as correlations (21), and scaled charged particle momentum distributions (22).

5.2 Technical status of the H1 experiment

Over the long running period of the H1-experiment and despite decreasing manpower in recent years the overall performance of the set-up has been continuously improved. For example the running efficiency from January to March 2007 reached 84 %. The HERA accounting starts with the luminosity tuning phase when both rings have been filled, the beams are at full energy and are brought into collision (62.3 pb^{-1} for this period). H1 starts to take data and tries to turn the tracking chambers on, when tuning is finished (59.7 pb^{-1} or 96 % remaining). This step depends critically on background conditions, which may vary from fill to fill, and apart from dead-time induced by readout, on-line analysis and data storage it accounts for most of the losses (53.5 pb^{-1} or 86 % left). Finally only 2% of the delivered luminosity is lost due to malfunctioning of the data acquisition, hardware components and errors of the shift crew, which was reduced to two persons from initially four. Many monitoring and operational tasks were automated over the years, e.g. the tracker turn on and trip recovery procedure (mostly caused by spikes in the beam, ageing effects have minor influence) and trigger prescale adjustment.

Benchmarks of HERA-II running are peak (average) luminosities of 37.5 (17.2) μb^{-2}s^{-1} and specific luminosities 1.79 (1.29) μb^{-2}s^{-1}mA^{-2} with maximum (average) proton and electron/positron currents of I_p=113 (93) mA and I_e=43 (27) mA, respectively. In 2006/7 (HERA-

ll) thus 0.59 pb^{-1} per day (excluding the annual shutdown period) were collected by H1 compared to 0.26 pb^{-1} per day in 1999/2000 (HERA-I). One has to admit that the original goal of the upgrade program calling for a factor of seven increase in peak luminosity with 74 $\mu b^{-2} s^{-1}$ expected has been missed, and that the time which was needed to reach routine operation after the end of HERA-I (2000-2003) was considerably underestimated.

Our group built a five-layer inner multiwire proportional chamber (CIP2000) for the upgraded H1-detector, which has finer granularity and increased redundancy, is equipped with state of the art electronics and an optical readout delivering signals for a sophisticated z-vertex trigger. It functioned without problems, and hence remained to be an essential ingredient of nearly all trigger elements. A technical description of the system and its performance has been submitted for publication (38). Other hardware improvements entered production modes in the last year: the liquid argon based jet trigger enhances the first-level trigger efficiency for low positron inelasticity, the match of this trigger with the fast track trigger derived from the central jet chamber enhances the sensitivity to $b-$quark physics at the third trigger level, and lastly a topological trigger derived from the backward electromagnetic calorimeter (SpaCal) which receives input also from the CIP2000 and the backward silicon tracker (BST) was implemented successfully. The latter will be useful for the low energy run (see Sec. 5.3).

In our annual report 2000/2001 at the end of the HERA-I period (3) we referred to the major effort of improving the calibration and alignment of all components of the tracker. The significant progress then achieved was based on the program *Millipede* (39; 40) developed by Volker Blobel of Hamburg University. It allows the determination of a large number of global detector parameters from a simultaneous linear least square fit of an arbitrary number of tracks accounting for the

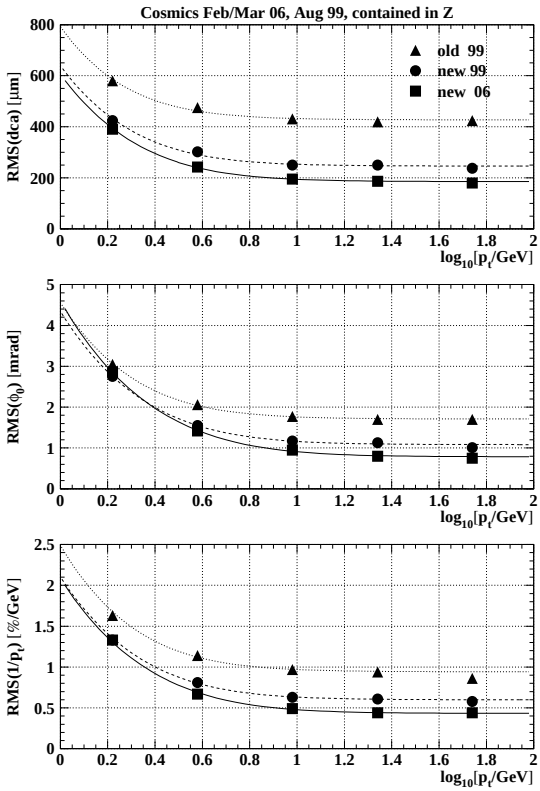

Figure 5.1: Track parameter resolution in the transverse plane obtained with the central jet chamber by comparing two halves of cosmic muon tracks traversing the central tracker. Shown as a function of the transverse momentum are the distance to the interaction point (dca), the azimuth (ϕ_0) and the curvature ($1/p_t$) in the 1999-data (HERA-I) before and after improvement of the code, and in the 2006-data (HERA-II) (from ref. [41]).

correlations with the local track parameters. This effort has continued and further improvements have been made for the HERA-II data. For example the radial and longitudinal variations of the electric and magnetic field in the central jet chamber (CJC), which influence drift velocity and Lorentz angle were implemented. The new elliptical shape of the central silicon tracker (CST) needed adjustments in the program apart from re-calibration, the $z-$information is now derived from CST and the central outer $z-$chamber (COZ) instead from the central inner $z-$chamber (CIZ) and

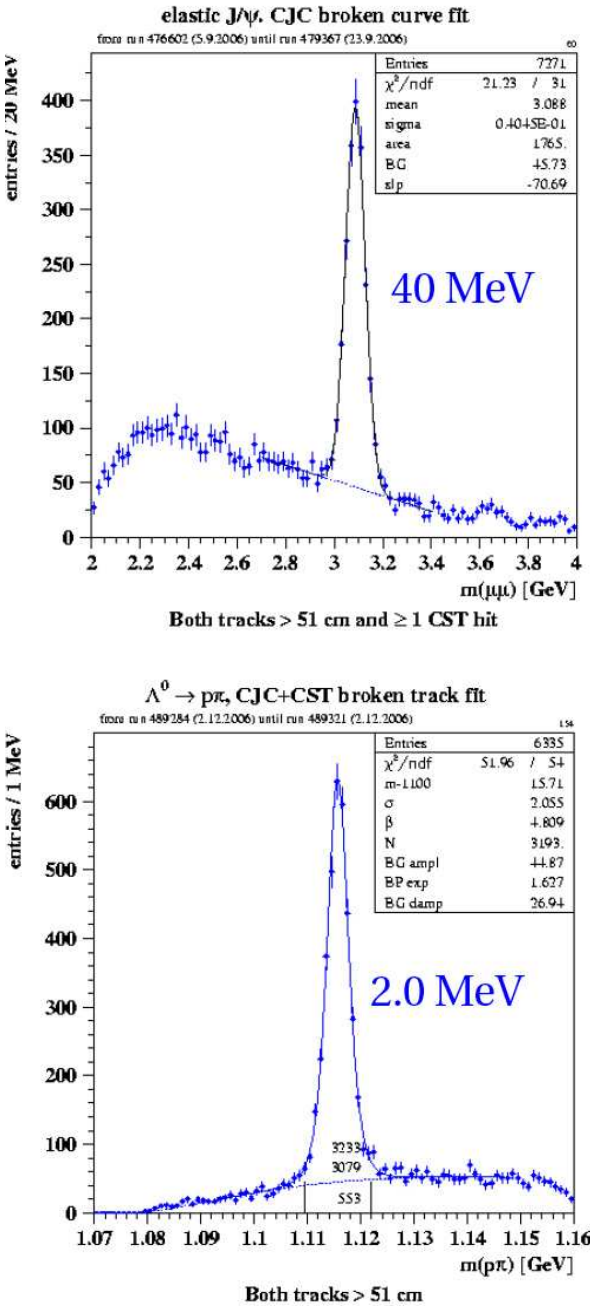

Figure 5.2:
Examples of the mass resolution obtained with the H1 central tracker after implementing the new broken-curve fit.
Top: J/Ψ decaying into a muon pair and bottom: Λ decaying into πp.
The r.m.s. widths of the peaks are indicated. Long tracks in the central jet chamber are required.

COZ, and charge division at both ends of the CJC wires. Figure 5.1, taken from a report at a recent LHC-workshop (41), summarizes the tracker performance in the transverse $R\varphi$ plane deduced from comparing the two halves of cosmic muon tracks traversing the central tracker. For momenta above 10 GeV/c, where the contribution from multiple scattering can be neglected a resolution for the distance of closest approach of 185 μm, for the track angle at the interaction vertex of 0.79 mrad and for the curvature ($1/p_t$) of 0.43%/GeV has been measured. The standard track fit does not allow for multiple scattering, it only corrects for the mean energy loss. The new fast track-fit algorithm based on broken lines (42) corrects for this, and leads to higher precision, as demonstrated by the r.m.s. width of the Λ and J/Ψ mass peaks shown in Fig. 5.2, which reduced from 2.5 to 2.0 MeV and from 43 to 40 MeV, respectively.

5.3 Low energy run

The H1 and the ZEUS collaboration expressed interest in low energy run with the HERA storage ring in September 2005. Considering the amount of e^+p-data taken since summer 2006, the observed evolution of the significance of the excess of observed high transverse momentum lepton events (see Sec. 5.4.1), the success of low energy machine studies earlier on, and the success of understanding high inelasticity data from standard running, the H1-collaboration requested a low energy run to start on March 21, 2007. This run has now successfully started. At a proton energy of 460 GeV a peak luminosity of 7.5 $\mu b^{-2}s^{-1}$ and a specific luminosities 0.46 $\mu b^{-2}s^{-1}mA^{-2}$ with 99 mA protons and 36 mA positrons have been reached, allowing for 0.1 to 0.2 pb^{-1} per fill.

The primary goal of the low energy run is the determination of the longitudinal structure function appearing in the inclusive deep

inelastic cross section as

$$\frac{d^2\sigma}{dxdQ^2} = \frac{2\pi\alpha^2 Y_+}{Q^4 x}\left[F_2(x,Q^2) - f(y)\cdot F_L(x,Q^2)\right] ,$$

with $y = Q^2/sx$, $Y_+ = 1+(1-y)^2$ and $f(y) = y^2/Y_+$. The two structure functions F_2 and F_L have so far not been properly disentangled at HERA. The measured cross sections have been interpreted in terms of F_2 with some reasonable assumptions on F_L, except at large y where the treatment was reversed (43). The two functions correspond to the transverse and longitudinal polarisation state of the exchanged virtual photon probing the proton structure, i.e. $F_T = F_2 - F_L$ and F_L, respectively. In the quark-parton model F_L is zero since longitudinally polarised photons do not couple to spin $1/2$ quarks (44). In the DGLAP approximation of perturbative QCD, to lowest order, the longitudinal structure function is given by (47)

$$F_L(x) = \frac{\alpha_s}{4\pi}x^2\int_x^1 \frac{dz}{z^3}\left[\frac{16}{3}F_2(z) + 8\sum e_q^2(1-\frac{x}{z})zg(z)\right]$$

with contributions from quarks and from gluons. At low x, $F_L(x,Q^2)$ essentially determines the gluon distribution $xg(x,Q^2)$ ($\approx 8.3F_L(0.4x)/\alpha_s$ numerically). Presently the gluon distribution at low x is constrained indirectly by the Q^2 evolution of $F_2(x,Q^2)$. This assumes the validity of the DGLAP theory, which becomes questionable at low x.

It is possible to extract the longitudinal structure function directly from two or more cross section measurements at fixed x and Q^2 by varying y, which is possible by changing s. Since $s = 4E_eE_p$ one may vary the electron or proton beam energy or both. The sensitivity to F_L is proportional to y^2. As at large y and low Q^2 the inelasticity is given by $y \approx 1-E'_e/E_e$, reducing the electron beam energy would require to lower the scattered electron energy below the 2 GeV trigger threshold. Moreover, a reduction of the electron beam energy affects the scattered electron angle stronger than a reduction of the proton beam energy would do. It has therefore been decided to opt for lowering E_p. Estimates for a successful determination of F_L to at least 5 standard deviations are based on the assumption, that 10 pb^{-1} can be collected at 460 GeV until the end of June 2007. At large y and low Q^2 the scattering kinematics at HERA resemble those of a fixed target scattering experiment: the electron scattered off quarks at very low x is scattered through a small angle. It is accompanied by part of the hadronic final state which is related to the struck quark. Since high inelasticities y demand to identify scattered electrons down to a few GeV of energy, there is a considerable background from hadrons or photons, e.g. from π^0 decay, usually from photoproduction with the scattered electron escaping unobserved through the beam pipe. Removal of this background is possible by requiring a track to be associated to the energy cluster in the SPACAL, which rejects photons, and by measuring its charge, which on a statistical basis allows the remaining part of the background to be removed, as was demonstrated with the BST and the CJC (43).

5.4 Results from recent analyses

5.4.1 High transverse momentum phenomena

Examining the data that H1 collected during the period 1994-2000, eighteen events were identified which contain an isolated electron or muon and show missing transverse momentum. The Standard Model (SM) predicted 12.4±1.7 events of this kind, the majority coming from the decays of W bosons. Whilst these numbers were broadly in agreement with each other, the comparison became more interesting when the selection was restricted to those events which have a particularly powerful jet. When this jet punched side-

Table 5.1: **Summary of the H1 searches for events with isolated electrons or muons of either charge with missing transverse momentum for all data sets taken up to February 2007, comprising 95% of the total integrated luminosity. The signal component of the Standard Model expectation, dominated by W production is indicated as well.**

H1-preliminary		Electron			Muon			Combined		
(Feb. 2007)		obs.	expected	signal	obs.	expected	signal	obs.	expected	signal
94-07 e^+p	Full sample	25	24.2±3.3	71%	13	6.3 ±1.0	85%	38	30.5±4.2	75%
258 pb^{-1}	$P_T^X > 25$ GeV	10	4.1 ±0.8	75%	8	3.7 ±0.6	85%	18	7.8 ±1.3	80%
98-06 e^-p	Full sample	16	19.4±2.7	65%	2	5.1 ±0.7	78%	18	24.4±3.4	68%
184 pb^{-1}	$P_T^X > 25$ GeV	3	3.8 ±0.6	61%	0	3.1 ±0.5	74%	3	6.9 ±1.0	67%
94-07 $e^\pm p$	Full sample	41	43.6±6.0	68%	15	11.4 ±1.7	82%	56	55.0±7.6	71%
442 pb^{-1}	$P_T^X > 25$ GeV	13	7.9 ±1.4	67%	8	6.8 ±1.1	79%	21	14.7±2.3	72%

ways (transversely) into the detector with a momentum of more than 25 GeV, ten events were found compared to a SM expectation of 2.9±0.5. The chance of a statistical fluctuation producing this number of observed events was around 0.15% (45). This exciting observation lead to the establishment of a hot line for events of this type, and allowed a continuous updating of the status. Table 5.1 summarizes the situation as it stood at the end of January 2007, an update of what was reported at the ICHEP2006 conference (32; 33). The statement *seemingly the HERA-II data are more SM like than the HERA-I data* captures the disappointing fact. The slight excess in the positron data is well compensated by the electron data (see also Fig. 5.3). A working group has been formed, which will combine the H1- and ZEUS data, which differ in their accepted kinematic range, but unfortunately also seem to hold no surprises either.

The general search for non-SM events following the method outlined in our 2004 publication (46) has been extended to the HERA-II data, too (37). All event topologies involving isolated electrons, photons, muons, neutrinos and jets with high transverse momenta are investigated in a single analysis. Events are assigned to exclusive classes according to their final state. A statistical algorithm is applied to search for deviations from the

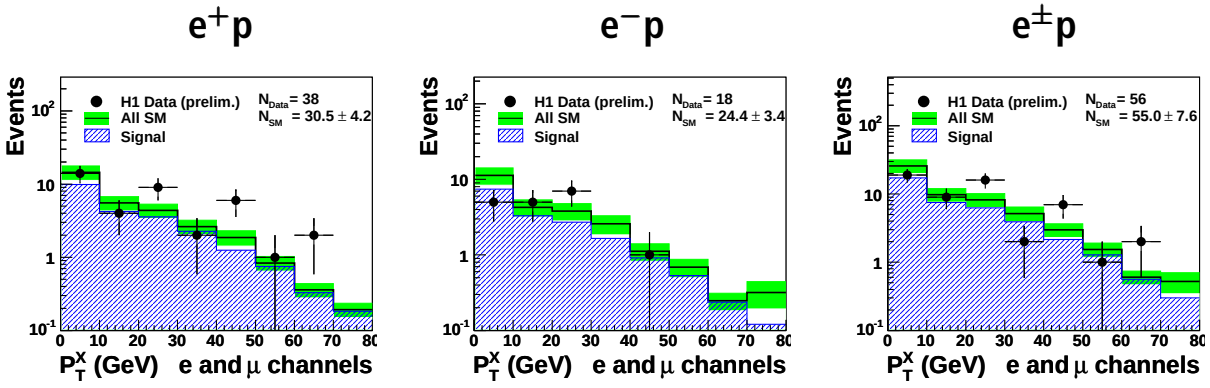

Figure 5.3: **The hadronic transverse momentum distribution in the combined electron and muon channels is compared to the Standard Model expectation (open histogram). The hatched histogram indicates the contribution of real W production which dominates the signal. The total number of observed and expected events are given by N_{Data} and N_{SM}, respectively. From left to right: e^+p, e^-p and combined data.**

Standard Model in the distributions of the scalar sum of transverse momenta or invariant mass of final state particles and to quantify their significance. No significant deviations from SM expectations have been found.

5.4.2 Isolated photons in photoproduction and deep inelastic scattering

Two thesis projects of Zürich graduate students concern the reaction $e^{\pm}p \to e^{\pm}\gamma X$ either with the exchanged virtual photon (Fig. 5.4) nearly on shell ($Q^2 \approx 0$, photoproduction (PP), thesis Krzysztof Nowak) or at higher momentum transfer ($Q^2 > 0$, deep inelastic scattering (DIS), thesis Carsten Schmitz). Common to both analyses is that the observed photon is isolated and has high transverse momentum (energy) E_T. In DIS the scattered electron is observed in the backward electromagnetic calorimeter of H1 (SpaCal), while in PP it escapes mostly unobserved through the beam pipe.

The reaction receives contributions from wide angle bremsstrahlung of the initial and final state electron or positron (LL) and from the radiation of the struck quark (QQ), and from their interference (LQ). The leading order diagrams are depicted in Fig. 5.4. In the QCD calculation of Gehrmann-de Ridder *et al* (4) pertaining to DIS the parton-level lepton-quark cross section $\hat{\sigma}(eq \to e\gamma q)$ is convoluted with the parton densities in the proton to obtain the $\sigma(ep \to e\gamma X)$ cross section. The most interesting QQ contribution is dominated by the direct radiation from the struck quark, but contains also the contribution from quark fragmentation to a photon. This part can not be calculated in perturbation theory (pQCD). A phenomenological process-independent quark-to-photon fragmentation function $D_{q\to\gamma}(z)$

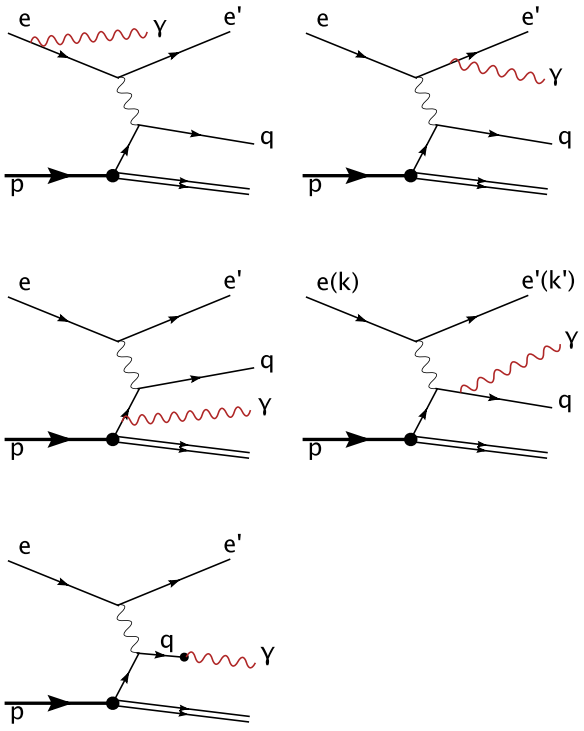

Figure 5.4: Leading order contributions to isolated photon production at $Q^2 \approx 0$ (photoproduction, PP) and for larger Q^2 (deep inelastic scattering, DIS). Top: initial and final state lepton bremsstrahlung in DIS; middle: radiation from the struck quark present in both DIS and PP; bottom: diagram illustrating the contribution from quark-to-photon fragmentation.

($z \equiv$ fraction of the quark momentum carried by the photon) is needed, for which data from LEP-experiments exist. Even at leading order, the parton-level cross section contains a collinear quark-photon divergence, which is absorbed into the fragmentation function. The reconstruction of the photon and the electron in different parts of the detector ensures sufficient separation to avoid collinear singularities in the LL QED-contribution. The interference term (LQ), which differs in sign for e^+p and e^-p scattering contributes less than 3 % to the cross section. The commonly used RAPGAP Monte Carlo generator (48) can also be used to predict the LL contribution, while for the QQ process the PYTHIA Monte Carlo generator (49) is available which, however,

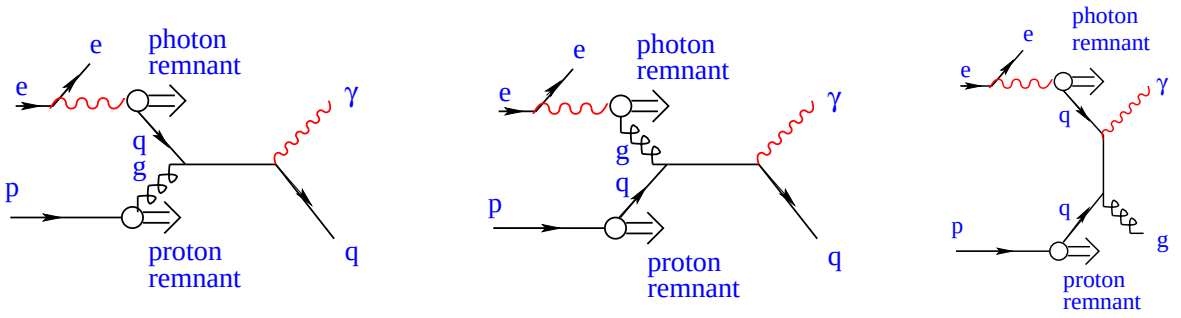

Figure 5.5: Resolved photon contribution to isolated photon production at $Q^2 \approx 0$.

does not contain the contribution from fragmentation, nor is the LQ-interference calculable in this way.

In photoproduction the direct QQ contribution described above is supplemented by the resolved photon contribution, where the photon converts itself into partons before it interacts (see Fig. 5.5). This contribution is available through PYTHIA, too.

Experimentally the DIS (PP) data are confined to the kinematic range in photon transverse energy: $3 < E_T^\gamma < 10$ GeV ($5 < E_T^\gamma < 10$ GeV), in pseudorapidity $\eta^\gamma \equiv -\ln\tan\theta^\gamma/2$: $-1.2 < \eta^\gamma < 1.8$ ($-1.0 < \eta^\gamma < 0.9$), in momentum transfer: $4 < Q^2 < 150$ GeV^2 ($Q^2 < 0.1$ GeV^2), in electron inelasticity: $0.05 < y < 0.9$ ($0.2 < y < 0.7$) and in the invariant mass of the hadronic system $W > 50$ GeV to exclude elastic Compton scattering. A typical DIS event is shown in Fig. 5.6. To ease the comparison with pQCD calculations an infrared-safe definition of the isolation criterion requires the fraction z of the jet energy carried by the photon to be larger than 0.9. In DIS the sample is divided further into subsamples without and with further jets.

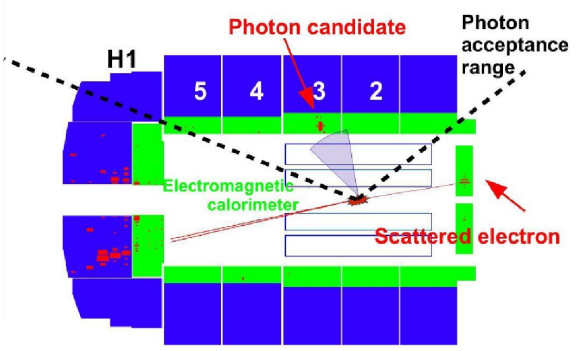

Figure 5.6:
An isolated high transverse momentum photon in a deep inelastic scattering event observed in the H1-detector. The kinematical acceptance is indicated.

The major challenge of the analysis is the discrimination of the photons, detected in the electromagnetic part of the liquid argon calorimeter, against π^0 and other mesons decaying into photons. The isolation criterion helps, since most π^0 appear as content of jets. But even after applying it, the background amounts to 70 % of the total sample. A multivariate analysis using six variables describing the spatial extent and symmetry of the shower in three dimensions is therefore used in the final discrimination step. This procedure was described in detail in last years annual report (3). As an example the signal extraction in the photoproduction data is shown in Fig. 5.7.

An excerpt of the preliminary photoproduction data is shown Fig. 5.8. Considering, that systematic errors have not been evaluated and not all cross checks have been done reasonable overall agreement with published, lower statistics results for the transverse energy dependence of the inclusive cross section is observed. The same holds for the comparison with theoretical predictions. Results for the η dependence and the photon plus jet cross section are available, too.

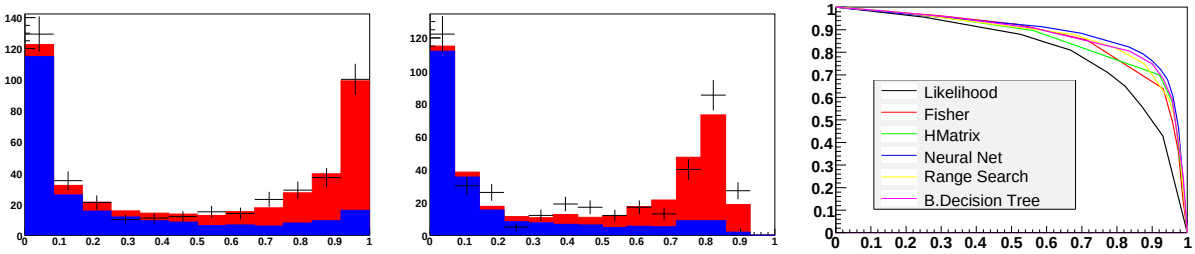

Figure 5.7: Photon signal extraction based on the analysis of shower shapes. The six electromagnetic cluster variables are either fed to a likelihood analysis (left), a neural network (middle) or four other commonly used multi-variate analysis methods (not shown). The background is represented by the blue histograms, the signal by the red histograms, the horizontal axis corresponds to the normalized discrimination variable. The signal selection efficiency (vertical axis) versus background rejection (horizontal axis) for all methods is shown on the right.

Examples of the measured DIS cross sections are shown in Figures 5.9 and 5.10. The difference in the angular distributions of the LL and the QQ radiation allows to disentangle the two contributions. Radiation from the electron is negligible for $\eta^\gamma > -0.6$. The leading order calculation (4) underestimates the inclusive cross section by 45 % most significantly at low Q^2. The same holds for the PYTHIA plus RAPGAP prediction, which lies 48 % lower. For $Q^2 > 40$ GeV^2 the leading order calculation is closer to the data (low by 25 %) and the shape is described well. Exclusive measurements of the cross section with and without additional jets are available for the first time, too. Radiation from the electron is largely suppressed for photon plus no jet. This separation has not been previously available. Both exclusive cross sections are underestimated by the leading order calculation, too, indicating the need for higher order calculation. The only previous measurement at HERA from the ZEUS-collaboration (51) only starts at $Q^2 \approx 35$ GeV^2, has a higher E_T-cut and considerably less statistics.

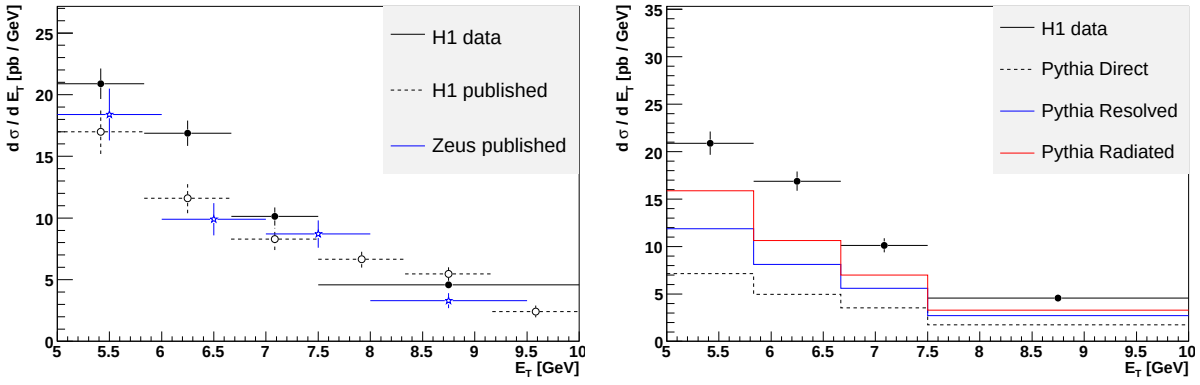

Figure 5.8: Preliminary results for the transverse momentum (energy) dependence of the inclusive cross section for isolated photon production compared to previous H1 and ZEUS photoproduction data (left) and to predictions using the PYTHIA Monte Carlo generator (right).

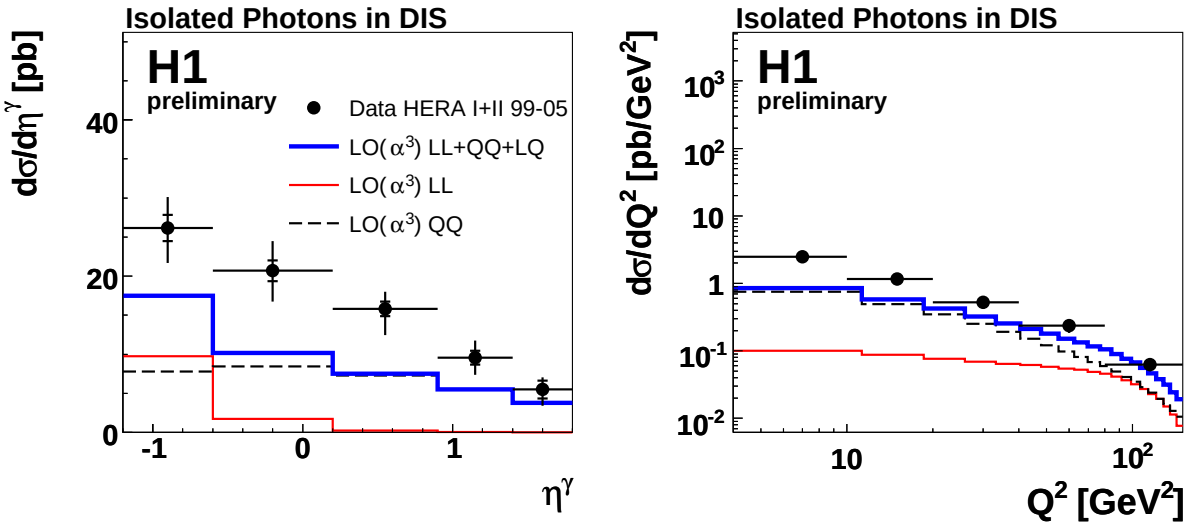

Figure 5.9: Inclusive differential cross sections $d\sigma/d\eta^\gamma$ and $d\sigma/dQ^2$ for isolated photons in DIS. The cross sections are shown together with a leading order $\mathcal{O}(\alpha^3\alpha_s^0)$ calculation [4] corrected for hadronisation effects, LL corresponding to radiation from the electron and QQ to radiation from the quark. LL is negligible for $\eta^\gamma > 0.6$. The calculation is low by 45% most significantly at low Q^2.

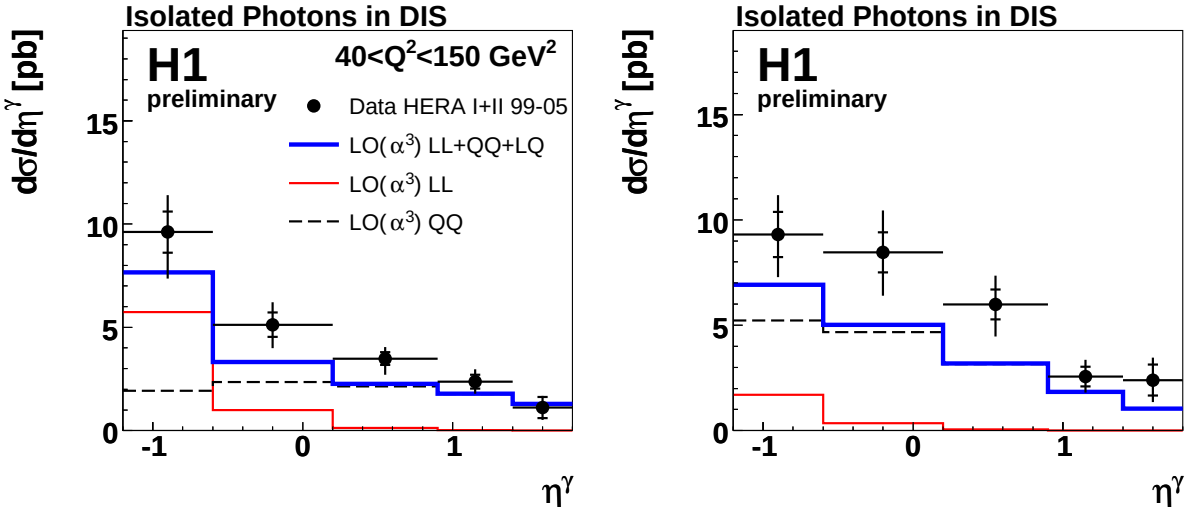

Figure 5.10: Differential cross sections $d\sigma/d\eta^\gamma$ for $Q^2 > 40$ GeV^2 (left) for the inclusive measurement and the exclusive measurement for photon plus no-jets with $Q^2 > 4$ GeV^2 (right). At high Q^2 there is much better agreement between calculation and measured data in shape and in magnitude. Exclusive sample: photon plus no jet: LO below the data but - compared to the inclusive sample - the radiation from the electron (LL) is suppressed, mainly by the W cut.

[1] **Search for Lepton Flavour Violation with the H1 Experiment at HERA**,
Linus Lindfeld, PhD Thesis, University of Zürich (2006).

[2] **Search for Lepton Flavour Violation in ep Collisions**,
H1-Coll., A. Aktas et al., DESY 07 – 007,
hep-ex/0703004, submitted to Eur.Phys.J.**C** (2007).

[3] Physik-Institut, University of Zürich,
Annual Reports 1996/7 ff.; available at
www.physik.unizh.ch/reports.html.

[4] A. Gehrmann-De Ridder, T. Gehrmann, and E. Poulsen,
Phys.Rev.Lett.**96** (2006), 132002;
Eur.Phys.J.**C47** (2006), 395.

[5] **Elastic J/ψ Production at HERA**,
H1-Coll., A. Aktas et al., DESY 05 – 161,
hep-ex/0510016, Eur.Phys.J.**C46** (2006), 585 - 603.

[6] **Photoproduction of Dijets with High Transverse Momenta at HERA**,
H1-Coll., A. Aktas et al., DESY 06 – 020,
hep-ex/0603014, Phys.Lett.**B639** (2006), 21 - 31.

[7] **Diffractive Photoproduction of ρ Mesons with Large Momentum Transfer at HERA**,
H1-Coll., A. Aktas et al., DESY 06 – 023,
hep-ex/0603038, Phys.Lett.**B638** (2006), 422 - 431.

[8] **Tau Lepton Production in ep Collisions at HERA**,
H1-Coll., A. Aktas et al., DESY 06 – 029,
hep-ex/060422, Eur.Phys.J.**C48** (2006), 699 - 714.

[9] **Search for Doubly-Charged Higgs Boson Production at HERA**,
H1-Coll., A. Aktas et al., DESY 06 – 038,
hep-ex/0604027, Phys.Lett.**B638** (2006), 432 - 440.

[10] **Measurement of Charm and Beauty Dijet Cross Sections in Photoproduction using the H1 Vertex Detector at HERA**,
H1-Coll., A. Aktas et al., DESY 06 –039,
hep-ex/0605016, Eur.Phys.J.**C47** (2006), 597 - 610.

[11] **Search for a Narrow Baryonic Resonance in Decaying in $K^0_s p$ or $K^0_s \bar{p}$ in Deep Inelastic Scattering at HERA**,
H1-Coll., A. Aktas et al., DESY 06 – 044,
hep-ex/060456, Phys.Lett.**B639** (2006), 202 - 209.

[12] **Diffractive Deep Inelastic Scattering with a Leading Proton at HERA**,
H1-Coll., A. Aktas et al., DESY 06 – 048,
hep-ex/0606003, Eur.Phys.J.**C48** (2006), 749 - 766.

[13] **Measurement and QCD Analysis of the Diffractive Deep Inelastic Scattering Cross Section at HERA**,
H1-Coll., A. Aktas et al., DESY 06 – 049,
hep-ex/0606004, Eur.Phys.J.**C48** (2006), 715 - 748.

[14] **Inclusive $D^{*\pm}$-Meson and $D^{*\pm}$-Jet Correlations in Photoproduction at HERA**,
H1-Coll., A. Aktas et al., DESY 06 – 110,
hep-ex/0608042, Eur.Phys.J.**C50** (2007), 251 - 269.

[15] **Diffractive Open Charm Production in Deep Inelastic Scattering and Photoproduction at HERA**,
H1-Coll., A. Aktas et al., DESY 06 – 164,
hep-ex/0610076, Eur.Phys.J.**C50** (2007), 1-20.

[16] **Search for Single Top Production in ep Collisions at HERA**,
Stefania Xella, Proc. Int. Workshop on Top Quark Physics (TOP2006), Coimbra, Portugal, January 12 - 15, 2006; Proc. of Science **TOP 2006** (2006), 030.

[17] **Production of D^* Mesons with Dijets in Deep Inelastic Scattering**,
H1-Coll., A. Aktas et al., DESY 06 – 240,
hep-ex/0701023, submitted to Eur.Phys.J.**C** (2007).

[18] **Tests of Factorisation in the Diffractive Production of Dijets in Deep Inelastic Scattering and Photoproduction at HERA**,
H1-Coll., A. Aktas et al., DESY 07 – 018,
hep-ex/0703022, submitted to Eur.Phys.J.**C** (2007).

[19] Contributed papers by the H1-Coll. to ICHEP2006: 33^{th} Int. Conf. on High Energy Physics Moscow (Russia), July 26-August 2, 2006; only those papers are listed, which have not yet been submitted to journals.

[20] **Threejet Production in Deep Inelastic ep Scattering and Low x Parton Dynamics at HERA** [19].

[21] **Azimuthal Correlations in Dijet Events from Deep Inelastic Electron-Proton Scattering at HERA** [19].

[22] **Scaled Charged Particle Momentum Distributions at High Q^2 at HERA** [19].

[23] **Inclusive Prompt Photon Production in Deep Inelastic Scattering at HERA** [19].

[24] **Determination of Diffractive Parton Densities by a Combined Analysis of Diffractive Dijet Production and of the Inclusive Diffractive Structure**

Function F_2^D in Deep Inelastic Scattering [19].

[25] **Measurement and Interpretation of Diffractive Cross Sections at Medium Q^2** [19].

[26] **Measurement of Deeply Virtual Compton Scattering at HERA-II** [19].

[27] **A New Measurement of Exclusive ρ^0 Meson Photoproduction at HERA** [19].

[28] **Charged Current Interactions in ep Scattering at HERA with Longitudinally Polarised Electrons** [19].

[29] **Neutral Current Interactions in $e^{\pm}p$ Scattering with Longitudinally Polarised Leptons** [19].

[30] **Search for Baryonic States Decaying to $\Xi\pi$ in Deep Inelastic Scattering at HERA** [19].

[31] **Diffractive Charm Production at HERA** [19].

[32] **Search for Events with Isolated Leptons and Missing Transverse Momentum** [19]; available at www-h1.desy.de/psfiles/confpap/ICHEP2006/-H1prelim-06-162.ps.

[33] **Multilepton Events at HERA** [19].

[34] **Search for Excited Neutrinos in e^-p Collisions at HERA** [19]

[35] **Search for Events with Isolated Tau-Leptons and Missing Transverse Momentum at HERA** [19]

[36] **Search for Leptoquarks in e^-p Collisions at HERA** [19]

[37] **A General Search for New Phenomena in e^-p Scattering at HERA** [19]; available at www-h1.desy.de/psfiles/confpap/ICHEP2006/-H1prelim-06-161.ps.

[38] **A Vertex Trigger based on Cylindrical Multiwire Proportional Chambers**,
J. Becker, K. Bösiger, L. Lindfeld, K. Müller, P. Robmann, S. Schmitt, C. Schmitz, S. Steiner, U. Straumann, K. Szeker, P. Truöl, M. Urban, A. Vollhardt, N. Werner, D. Baumeister, S. Löchner, and M. Hildebrandt, physics/0701002, submitted to Nucl.Instr.Meth. A (2007).

[39] **A New Method for the High Precision Alignment of Track Detectors**,
Proc. Conf. on Advanced Statistical Techniques in Particle Physics, Durham, UK (Mar. 18-22, 2000), M.R. Walley and L. Lyons eds., p. 268; DESY 02 – 077, hep-ex/0208021.

[40] **Software Alignment for Tracking Detectors**,
Proc. Workshop on Tracking in High Multiplicity Environments (TIME05), Zürich (Oct. 3-7, 2005), Nucl.Instr.Meth. A**566** (2006), 5.

[41] **H1 Alignment Experiences**,
C. Kleinwort, Contr. to LHC-Detector Alignment workshop, CERN, Geneva (Sept. 4-6, 2006), to be published in CERN Yellow Reports.

[42] **A New Fast Track-Fit Algorithm Based on Broken Lines**,
Proc. Workshop on Tracking in High Multiplicity Environments (TIME05), Zürich (Oct. 3-7, 2005), Nucl.Instr.Meth. A**566** (2006), 14.

[43] **Measurement of Inclusive ep Scattering at Low and a Determination of α_s**,
H1-Coll., A. Adloff et al., Eur.Phys.J.**C21** (2001), 33; Rainer Wallny, PhD Thesis, University of Zürich (2001); see also H1-report H1prelim-03-043 available at www-h1.desy.de/general/home/intra_home.html

[44] G. Callan, and D. Gross, Phys.Rev.Lett.**22** (1969), 156.

[45] **Isolated Electrons and Muons in Events with Missing Transverse Momentum at HERA**,
H1-Coll.. V. Andreev et al., Phys.Lett.**B561** (2003), 241;
Observation of Events at Very High Q^2 in ep Collisions at HERA,
H1 Collab., C. Adloff et al., Z.Phys. **C74** (1997), 191.

[46] **A General Search for New Phenomena in ep Scattering at HERA**,
H1 Collab., A. Aktas et al., Phys.Lett.**B602** (2004), 14.

[47] G. Altarelli, and G. Martinelli, Phys.Lett.**B76** (1978), 89.

[48] H. Jung, Comp. Phys. Comm. **86** (1995), 147 (Version 3.1); see also www.desy.de/jung/rapgap.html

[49] T. Sjöstrand, L. Lönnblad, and S. Mrenna, PYTHIA 6.2: Physics and manual, Lund University rep. LU-TP-01-21 (2001); hep-ph/0108264.

[50] **Measurement of Prompt Photon Cross Sections in Photoproduction at HERA**,
H1-Coll., A. Aktas et al., Eur.Phys.J.**C38** (2005), 437.

[51] ZEUS-Coll.: S. Chekanov et al., Phys.Lett.**B595** (2004), 86; Eur.Phys.J.**C49** (2007), 511; J. Breitweg et al. Phys.Lett.**B472** (2000), 175.